592 Journal of Electrical Engineering & Technology Vol. 5, No. 4, pp. 592~596, 2010
DOI: 10.5370/JEET.2010.5.4.592

Characteristic Analysis for IPMSM Considering Flux-Linkage Ripple

Dong-Kyun Woo†, Sang-Yeop Kwak*, Jang-Ho Seo* and Hyun-Kyo Jung*

Abstract – In a multi-layer interior permanent magnet synchronous motor, the *d*- and *q*-axis parameters vary nonlinearly according to different load conditions, consequently changing the level of saturation. The flux-linkage of *d*- and *q*-axis conveys ripple characteristics resulting from mechanical structure and degree of magnetic saturation. If the calculated flux-linkage is correct, the torque using the Maxwell stress tensor method is the same torque calculated by the flux-linkage. However, discrepancy between results exists. In this paper, the *d*- and *q*-axis flux-linkage, in consideration of the ripple characteristic, is calculated. Simulation results are then compared with experimental results.

Keywords: Flux-linkage, IPMSM, Motor, Parameter, Ripple

1. Introduction

The interior permanent magnet synchronous motor (IPMSM) has many advantages, such as high power density and wide speed range, due to its salient rotor structure [1]. The multi-layer IPMSM adopting a multi-layer structure in rotor offers additional reluctance torque given its large saliency. The multi-layer IPMSM can also provide additional improved characteristics, such as high starting torque and constant power operation, in the wide speed range by using field weakening control [2], [3]. However, in order to control this device, predicting the accurate machine parameters in the design stage is necessary [4].

In the multi-layer IPMSM, *d*- and *q*-axis parameters vary nonlinearly according to different load conditions, consequently changing the level of saturation.

The flux-linkage of *d*- and *q*-axis presents a ripple characteristic resulting from mechanical structure and degree of magnetic saturation. For superior performance, a multi-layer IPMSM should be operated in a magnetic saturation region.

The aforementioned problem was investigated using a previously proposed analysis and an experimental method that calculates the *d*- and *q*-axis flux-linkage in multi-layer IPMSM. In this paper, the analysis method used to calculate the flux-linkage, with specific focus on the ripple characteristic, is presented.

2. Analysis Model

The analysis model presented in this paper is a multi-layer IPMSM characterized by a high power density and wide speed range. Fig. 1 shows the cross-sectional view of the analysis model.

In the rotor structure, permanent magnets are partially embedded into each layer in order to obtain the sinusoidal back-EMF waveform. The design specification of the analysis model is summarized in Table 1.

Fig. 1 shows two different flux paths and a magnetic reluctance difference generated in *d*- and *q*-axis. The reluctance difference of the two axes is used to attain the high power density and the extended speed range during motor operation.

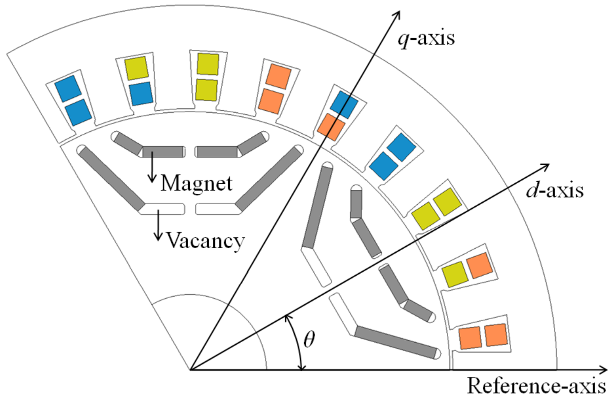

Fig. 1. Analysis model.

Table 1. Design specifications

Number of poles		6
Number of slots		27
Stacking length [mm]		230
Stator inner diameter [mm]		172
Stator outer diameter [mm]		240
Rotor inner diameter [mm]		50
Rotor outer diameter [mm]		170
Power	Rated power [kW]	50
	Maximum power [kW]	100
Maximum torque [Nm]		300
Maximum speed [rpm]		12000

† Corresponding Author: Dept. of Electrical Engineering, Seoul National University, Korea.(underdamp@snu.ac.kr)
* Dept. of Electrical Engineering, Seoul National University, Korea.(underdamp@snu.ac.kr)
Received: February 27, 2010; Accepted: April 5, 2010

3. Previous Method of Analysis

The flux-linkage can be calculated by

$$\lambda_d = \frac{2}{3}[\cos(\theta_e)\lambda_a + \cos(\theta_e - \frac{2}{3}\pi)\lambda_b + \cos(\theta_e + \frac{2}{3}\pi)\lambda_c] \quad (1)$$

$$\lambda_q = \frac{2}{3}[-\sin(\theta_e)\lambda_a - \sin(\theta_e - \frac{2}{3}\pi)\lambda_b - \sin(\theta_e + \frac{2}{3}\pi)\lambda_c] \quad (2)$$

where λ_d and λ_q are *d*- and *q*-axis flux-linkage; λ_a, λ_b, and λ_c are the flux-linkages per phase; and the rotor positional angle θ_e is the electrical angle between the *d*-axis and reference axis, as shown in Fig. 1 [5]. Previous analysis involved a fixed angle between two references, and hence, calculation was conducted on the flux-linkage based only on the change in current angle. If the calculated flux-linkage were correct, the torque T_s using the Maxwell stress tensor method would be the same as torque T_e. This can be calculated by

$$T_e(i_d, i_q) = \frac{3}{2}\frac{P}{2}[\lambda_d(i_d, i_q)i_q - \lambda_q(i_d, i_q)i_d] \quad (3)$$

where i_d and i_q are *d*- and *q*-axis currents, and *P* is the number of poles. However, dissimilarity was observed in the two analysis results, as well as discrepancy in the different rotor positions. Fig. 2 shows the comparative result between T_s and T_e according to the current angle. The result implies that the previous analysis method has not reflected the electromagnetic characteristics accurately. Table 2 shows an error of about 30 Nm between the calculated torque results when the current angle was considered.

Fig. 3 shows the characteristics of the torque ripple based on the change in rotor position at different current angles. Fig. 4 and Fig. 5 present the flux-linkage variation for the torque ripple period in Fig. 3. As shown by results presented in from Fig. 3 to Fig. 5, torque ripple and flux-linkage variation were within the same period. The T_s generated with a specified current is presented as an average torque T_{s_avg} for a period of torque ripple. Therefore, in this paper, the same method was applied in the flux-linkage calculation.

Table 2. Torque results according to current angle

Current angle [deg]	120	150	175
T_{s_avg} [Nm]	360.3	358.4	74.9
T_{s_diff} [Nm]	26.1	31.7	30.6
Torque ripple [%]	7.2	8.8	40.8

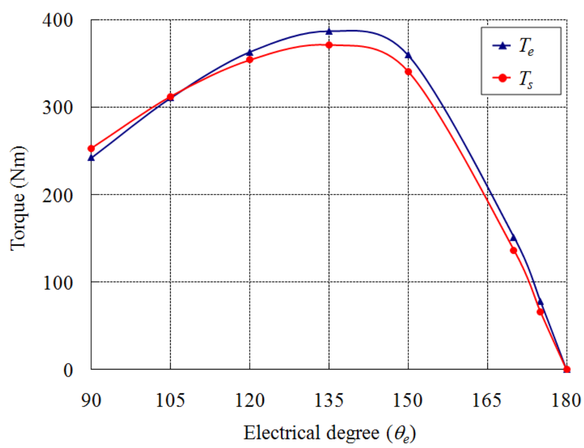

Fig. 2. Comparison between T_s and T_e according to current angle ($\theta_m = 0°$, $i_{peak\text{-}to\text{-}peak} = 640$ A).

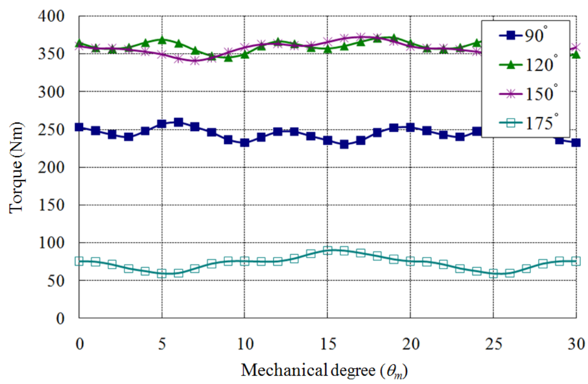

Fig. 3. Torque ripple characteristics according to change in rotor position at different current angles.

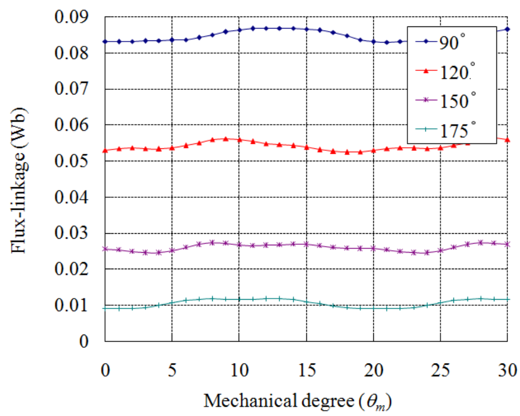

Fig. 4. Ripple characteristics of *d*-axis flux-linkage.

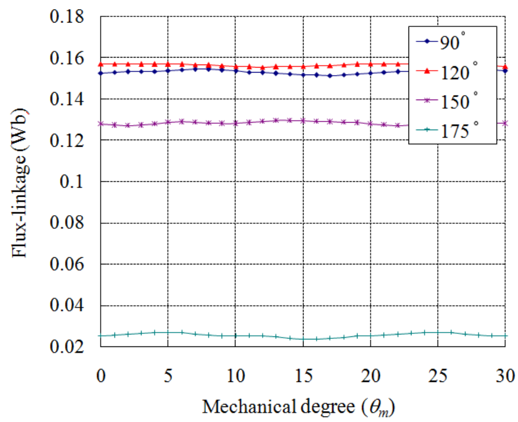

Fig. 5. Ripple characteristics of *q*-axis flux-linkage.

4. Flux-Linkage Calculation and Ripple Characteristics

Flux-linkage was calculated based on the change in rotor position. The angle between two reference frames would change with rotor rotation. The flux-linkages for each angle were calculated while the rotor was operating. Table 3 presents the ripple characteristics of the flux-linkage and its corresponding values for torque ripple. The table also shows similar torque ripples and flux-linkage ripple characteristics for different current angles.

In this paper, the d- and q-axis flux-linkage are introduced, taking into account the ripple characteristics:

$$\lambda_d^*(i_d, i_q) = \frac{\sum_{\theta=0}^{N-1} \lambda_d(i_d, i_q, \theta)}{N} \tag{4}$$

$$\lambda_q^*(i_d, i_q) = \frac{\sum_{\theta=0}^{N-1} \lambda_q(i_d, i_q, \theta)}{N} \tag{5}$$

where N is the number of calculation point during the period of flux-linkage ripple. Based on the average flux-linkage for a ripple period, the average torque T_{e_avg} can then be analyzed by

$$T_{e\_avg}(i_d, i_q) = \frac{3}{2}\frac{P}{2}[\lambda_d^*(i_d, i_q) i_q - \lambda_q^*(i_d, i_q) i_d] \tag{6}$$

5. Evaluation of the Proposed Method

The voltage equation for the IPMSM is presented by

$$V_d = i_d R_s + L_d \frac{di_d}{dt} - \omega\lambda_q \tag{7}$$

$$V_{qs} = i_q R_s + L_q \frac{di_q}{dt} + \omega\lambda_d \tag{8}$$

where V_d and V_q are the d- and q-axis components of terminal voltage; L_d and L_q are the inductances along d- and q-axis; and R_s is the armature winding resistance.

Since the measurement was conducted in the steady state, derivative terms were neglected. Therefore, λ_d and λ_q can be defined by

$$\lambda_d = \frac{V_q - i_q R_s}{\omega}, \qquad \lambda_q = -\frac{V_d - i_d R_s}{\omega} \tag{9}$$

However, R_s includes both phase and system resistance. To avoid measurement errors for flux-linkage from R_s in (9), voltage equations were employed. The voltage equations corresponding to both generating and motoring modes were calculated as

$$V_d^+ = i_d R_s - \omega L_q i_q = i_d R_s - \omega\lambda_q \tag{10}$$

$$V_q^+ = i_q R_s + \omega(L_d i_d + \lambda_f) = i_q R_s + \omega\lambda_d \tag{11}$$

$$V_d^- = i_d R_s + \omega L_q i_q = i_d R_s + \omega\lambda_q \tag{12}$$

$$V_q^- = -i_q R_s + \omega(L_d i_d + \lambda_f) = -i_q R_s + \omega\lambda_d \tag{13}$$

where V_d^+ and V_q^+ are the d- and q-axis voltages measured in the motoring mode; V_d^- and V_q^- are the d- and q-axis voltages measured in the generating mode; and λ_f is the maximum flux linkage of the permanent magnet [6]. In both motoring and generation modes, the same magnitude of d- and q-axis current excitations would occur; the same magnetic saturation would also be distributed in the motor. Based on (10)-(13), the d- and q-axis flux-linkage can be expressed by

$$\lambda_q = \frac{V_d^- - V_d^+}{2\omega}, \qquad \lambda_d = \frac{V_q^- + V_q^+}{2\omega} \tag{14}$$

Fig. 6 shows the prototype motor used to verify the proposed analysis method. From Fig. 7 to Fig. 10, the graphs show the comparative results for the proposed method and the experiment of the prototype motor. Based on these results, the torque and parameters corresponding to the combined currents in the multi-layer IPMSM were then evaluated as an average value while considering the ripple characteristics. Furthermore, in this paper, the mechanical characteristics and magnetic saturation were both taken into account in the proposed method for the d- and q-axis flux-linkage calculation.

(a) (b)

Fig. 6. Configuration of prototype motor: (a) stator and (b) rotor.

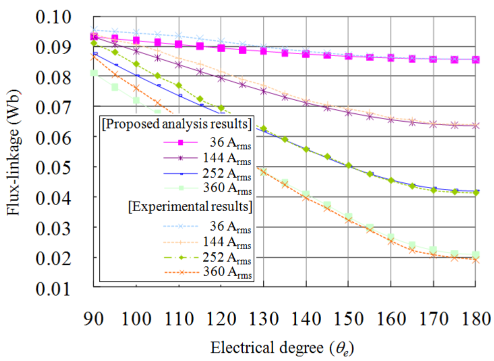

Fig. 7. Comparison between the proposed analysis and experimental results for the d-axis flux-linkage.

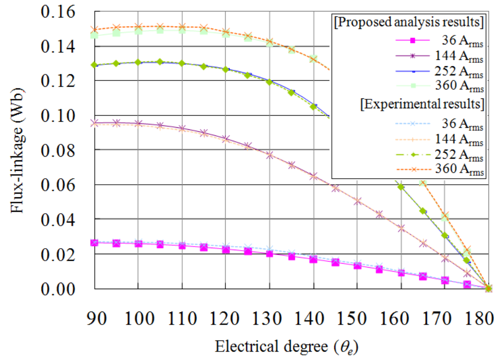

Fig. 8. Comparison between the proposed analysis and experimental results for the q-axis flux-linkage.

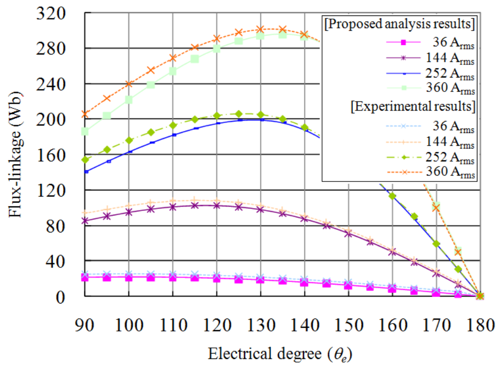

Fig. 9. Comparison between the proposed analysis and experimental results for the torque.

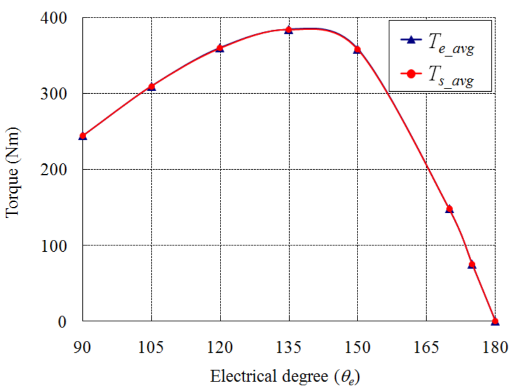

Fig. 10. Comparison between T_{s_avg} and T_{e_avg} according to the current angle ($i_{peak\text{-}to\text{-}peak}$ = 640A).

6. Conclusion

In this paper, we presented that the flux-linkage which is one of the most important parameters in an IPMSM has ripple characteristics as the rotor rotates. A method of calculating the flux-linkage variation using finite element analysis is suggested. Moreover, the behavior of the flux-linkage variation is analyzed with taking account of magnetic saturation and the mechanical structure.

Acknowledgement

This research was supported by a grant (Code07 Next Generation High Speed Train A01) from Railroad Technology Development Program (RTDP) funded by Ministry of Land, Transport and Maritime Affairs of Korean government.

References

[1] R. Y. Tang, “Modern permanent magnet machines theory and design,” Beijing, China Machine Press, 1997.

[2] G. X. Zhou, R. Y. Tang, D. H. Lee, and J. W. Ahn, “Field circuit coupling optimization design of the main electromagnetic parameters of permanent magnet synchronous motor,” *JEET*, Vol. 3, No. 1, pp. 88-93, Mar. 2008.

[3] Jang-Ho Seo, Chang-Hwan Im, Sang-Yeop Kwak, Cheol-Gyun Lee, and Hyun-Kyo Jung, “An Improved Particle Swarm Optimization Algorithm Mimicking Territorial Dispute Between Groups for Multimodal Function Optimization Problems,” *IEEE Trans. Magn.*, Vol. 44, No. 6, pp. 1046-1049, Jun. 2008.

[4] E. Levi, “Saturation modeling in dq axis models of salient pole synchronous machines,” *IEEE Trans. Energy Conversion*, Vol. 14, No. 1, pp. 44-50, Mar. 1999.

[5] J. R. Hendershot, and T. J. E. Miller, “Design of Brushless Permanent Magnet Motors,” Oxford, 1994.

[6] B. Stumberger, G. Stumberger, D. Dolonar, A. Hamler, and M. Trlep, “Evaluation of saturation and cross-magnetization effects in interior permanent-magnet synchronous motor”, *IEEE Trans. Ind. Appl.*, Vol. 39, No. 5, pp. 1264-1271, Oct. 2003.

Dong-Kyun Woo received B.S degree in electrical engineering from Yonsei university, Seoul, Korea, in 2007. His research interests are numerical analysis and design of electrical machines.

Sang-Yeop Kwak received Ph.D. degree in electrical engineering from the Seoul National University, Seoul, Korea, in 2008. His current research is focused on the design of electrical machines.

Jang-Ho Seo received Ph.D. degree in electrical engineering from the Seoul National University, Seoul, Korea, in 2010. His research interests are numerical analysis and design of electrical machines.

Hyun-Kyo Jung received Ph.D. degree in electrical engineering from Seoul National University. His research interests are electric machinery, EM waves, circuit breakers, and so on.